Supporting Information

Hierarchical VN/Co_3ZnC@NCNTs composite as a multifunctional integrated host for lithium-sulfur batteries with enriched adsorption sites and accelerated conversion kinetics

Junjie Fu,[a] Zewei Shen,[a] Daoping Cai,[a]* Ban Fei,[a,d] Chaoqi Zhang,[b,c] Yaguang Wang,[a] Qidi Chen,[a] and Hongbing Zhan[a]*

[a] College of Materials Science and Engineering, Fuzhou University, Fujian 350108, China.

[b] Catalonia Institute for Energy Research - IREC, Sant Adrià de Besòs, Barcelona, 08930, Spain.

[c] Department of Electronic and Biomedical Engineering, Universitat de Barcelona, 08028, Barcelona, Spain.

[d] School of Chemistry, Trinity College Dublin, Dublin 2, Ireland.

*Corresponding authors: Daoping Cai and Hongbing Zhan.

E–mail addresses: dpcai@fzu.edu.cn and hbzhan@fzu.edu.cn.

Experimental Section

Synthesis of $Co_2V_2O_7$ precursor. The $Co_2V_2O_7$ precursor was synthesized via a simple water bath reaction. Typically, 0.234 g of NH_4VO_3 was dissolved in 40 mL of deionized water with incessant stirring for 10 min at 70 °C to form a canary yellow solution. Afterwards, 0.095 g of $CoCl_2 \cdot 6H_2O$ and 1.2 g of hexamethylenetetramine (HMTA) were added into the canary yellow solution successively with continuous stirring for 4 h at 80 °C. After cooling to room temperature, the material was washed several times with deionized water and ethanol and then dried at 70 °C for 12 h.

Synthesis of $Co_2V_2O_7$@ZIF-8 heterostructure. In a typical preparation, 0.01 g of $Co_2V_2O_7$, 0.73 g of $Zn(NO_3)_2 \cdot 6H_2O$ and 1.0 g of polyvinylpyrrolidone (PVP) were dispersed in 20 mL of methanol successively by ultrasonication for 5 min to form solution A. Subsequently, solution B was prepared by dissolving 0.82 g of 2-methylimidazole in another 20 mL of methanol with continuous stirring. Afterwards, the solution B was added into the solution A gradually and then stirred for 10 min at room temperature to form the $Co_2V_2O_7$@ZIF-8 heterostructure. Finally, the sample was washed repeatedly with ethanol and then dried at 70 °C for 12 h.

Synthesis of VN/Co_3ZnC@NCNTs and VN/Co@NCNTs composites. VN/Co_3ZnC@NCNTs and VN/Co@NCNTs composites were synthesized by melamine-assisted nitridation. Typically, a porcelain boat holding $Co_2V_2O_7$@ZIF-8 was placed in the downstream position of horizontal quartz tube furnace and a porcelain boat containing 3.0 g of melamine powder was put into the upstream position separately. Then the $Co_2V_2O_7$@ZIF-8 heterostructure was heated to 600 °C with a heating rate of 5 °C min^{-1} in mixture gas (95% Ar, 5% H_2) and held for 2 h to acquire the hierarchical VN/Co_3ZnC@NCNTs composite. The VN/Co@NCNTs composite was synthesized through a similar procedure by nitriding the $Co_2V_2O_7$ precursor.

Synthesis of S@VN/Co_3ZnC@NCNTs, S@VN/Co@NCNTs, S@$Co_2V_2O_7$ and S@Super P composites. Sulfur encapsulation was performed by a melt-diffusion method. VN/Co_3ZnC@NCNTs was manually mixed with the sulfur powder in a mass ratio of 1:3 in an agate mortarm, and then the mixture was heated at 155 °C for 12 h

in order for the molten sulfur to infiltrate into VN/Co_3ZnC@NCNTs. The sample was cooled down to room temperature and the final product S@VN/Co_3ZnC@NCNTs composite was obtained. The S@VN/Co@NCNTs, S@$Co_2V_2O_7$ and S@Super P composites were prepared using the similar method.

Materials characterization. X-ray diffractometer (XRD, D/maxUltimaIII Rigaku, Cu Kα radiation, λ = 0.15418 nm), X-ray photoelectron spectroscopy (XPS, Thermo Fisher Scientific, ESCALAB 250), field emission scanning electron microscope (FESEM, Germany, Zeiss Supra55) and high-resolution transmission electron microscope (HRTEM, FEI, Talos F200i) were performed to determine the detailed information of composition, microstructure and morphology of the products. The thermogravimetric analysis (TGA, NETZSCH, STA449-F5) was carried out in the temperature range of 25 to 600 °C at a heating rate of 10 °C min^{-1} under N_2 atmosphere to record the content of sulfur in synthesized products.

Electrochemical measurements. For assembling Li-S cells, the cathode slurry was acquired via mixing 70 wt% active materials (S@VN/Co_3ZnC@NCNTs, S@VN/Co@NCNTs, S@$Co_2V_2O_7$ or S@Super P), 20 wt% Super P and 10 wt% polyvinylidene fluoride (PVDF) in N-Methylpyrrolidone (NMP) solvent. The slurry was coated on carbon coated aluminum foil and then the carbon coated aluminum foil with dried slurry was cut into circle disks with a parameter of 12 mm after vacuum drying at 60 °C for 6 h. The areal sulfur mass loading for each disk was about 1.0-1.2 mg cm^{-2} for the typical electrochemical measurements. Cathode with high sulfur mass loading of about 4.5 mg cm^{-2} was employed via coating the slurry mentioned above on carbon paper and dried at 60 °C under vacuum overnight. CR2032 coin cells were assembled in the glovebox under an argon gas atmosphere to measure electrochemical properties. The disk made from active materials (S@VN/Co_3ZnC@NCNTs, S@VN/Co@NCNTs, S@$Co_2V_2O_7$ or S@Super P) and the lithium foil were employed as working and counter electrodes, respectively, and the Celgard 2400 was used as the separator. The electrolyte was 1.0 M bis(trifluoromethanesulfonyl)imide lithium salt (LiTFSI) in 1,2-dimethoxyethane (DME) and 1,3-dioxolane (DOL) (1:1 in volume) solution containing 1.0 wt% $LiNO_3$. The electrolyte/sulfur ratio was approximately 30

μL mg^{-1} for all prepared Li-S cells, and 8 μL mg^{-1} for high-loading coin cell. The galvanostatic charge/discharge (GCD) test and rate performance were tested by a battery test system (LAND CT2001A) within a voltage range from 1.7 to 2.8 V. Cyclic voltammetry (CV) curves and electrochemical impedance spectroscopy (EIS) were measured by electrochemical workstation (CHI660E). CV curves were performed with the sweep rates from 0.1 to 0.5 mV s^{-1}. EIS profiles were tested with the frequency range from 10^{-2} to 10^{5} Hz.

DFT calculations. The DFT calculations were carried out using Vienna Ab initio Simulation Package (VASP). The Projected Augmented Wave (PAW) methods was used to process the core states, and the exchange and correlation terms were described by Perdew-Burke-Ernzerh (PBE) functional with the generalized gradient approximation (GGA). For all the calculations, about 15 Å vacuum layer was applied to prevent the vertical interactions between slabs. The Brillouin zone integration is carried out using a k-point mesh satisfied ka~30 Å in different models. The DFT-D3 method of Grime was adopted in all the calculations to evaluate the van der Waals interactions. Herein, the (111) surface of Co and (111) surface of Co_3ZnC were used as the catalytic interface, those surfaces were abundantly exposed in experimental situations. The binding energy for Li_2S_6 on Co and Co_3ZnC substrates were defined in the following equation:

$$\Delta Gads=G(ads)-G(slab)-G(Li_2S_6)$$

where the G(ads) refers to the total energy after Li_2S_6 absorbtion, G(slab) refers to the energy of different slabs and $G(Li_2S_6)$ refer to the energy of Li_2S_6, respectively.

Lithium polysulfide adsorption tests. Li_2S_6 solution (0.1 M) was prepared via mixing sulfur and lithium sulfide (99.9%, Alfa Aesar) in a molar ratio of 5:1 in DOL/DME solution (1:1 in volume) followed by stirring vigorously at 70 °C for 24 h until a dark brown solution was formed. Then the same weight (20 mg) of VN/Co_3ZnC@NCNTs, VN/Co@NCNTs, $Co_2V_2O_7$ and Super P were added into 3 mL Li_2S_6 solution (5 mM), respectively. All operations were carried out in glove box filled with argon atmosphere.

Symmetric cell assembly and measurements. Li_2S_6 solution (0.25 M) was prepared

by vigorous stirring sulfur and lithium sulfide (99.9%, Alfa Aesar) in a molar ratio of 5:1 in the electrolyte (1.0 M LiTFSI in DOL/DME (1:1 in volume)) at 70 ℃ for 24 h. The electrode was prepared via mixing active materials (VN/Co_3ZnC@NCNTs, VN/Co@NCNTs or $Co_2V_2O_7$) and PVDF with a weight ratio of 9:1 in NMP solvent followed by coating the slurry onto aluminum foil, ensuring the mass loading is approximately 1.0 mg cm^{-2}. CR2025 coin cells were assembled in the glovebox under an argon atmosphere to test electrochemical properties of symmetric cells. Two identical electrodes were used as the working and the counter electrodes, and the Celgard 2400 was used as the separator. 40 μL of Li_2S_6 (0.25 M) was used as electrolyte. CV curves were measured by electrochemical workstation (CHI660E) at a scan rate of 5 mV s^{-1} in a potential window of −1.0 to 1.0 V.

Li_2S nucleation tests. Li_2S_8 solution (0.5 M) was prepared via mixing sulfur and lithium sulfide (99.9%, Alfa Aesar) in a molar ratio of 7:1 and dissolving the mixture in DME and DOL (1:1 in volume) solution containing 1.0 M LiTFSI under vigorous stirring for 24 h. Carbon papers (CP) were used as current collector to load the VN/Co_3ZnC@NCNTs, VN/Co@NCNTs or $Co_2V_2O_7$. VN/Co_3ZnC@NCNTs, VN/Co@NCNTs and $Co_2V_2O_7$ were dispersed in ethanol under ultrasonic, respectively, and then added dropwise onto CP. The average mass loading is approximately 0.6 mg cm^{-2}. Nucleation of Li_2S was conducted in CR2032 coin cells. 20 μL of Li_2S_8 (0.5 M) was dropped onto the CP side, and 20 μL of blank electrolyte with 1.0 M LiTFSI and 1 wt% $LiNO_3$ was dropped onto the lithium foil side. For Li2S nucleation, the cells were first discharged at a current of 0.112 mA to 2.19 V and then hold the voltage at 2.05 V until the current decreased to 10^{-2} mA for Li_2S nucleation and growth.

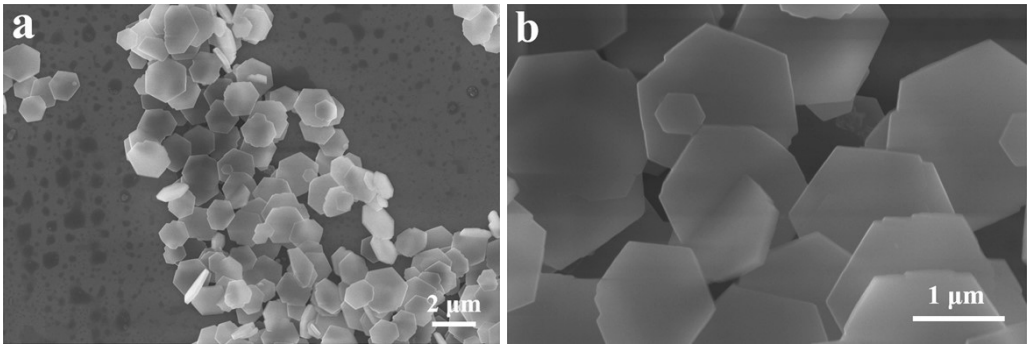

Fig. S1. SEM images of the $Co_2V_2O_7$ precursor.

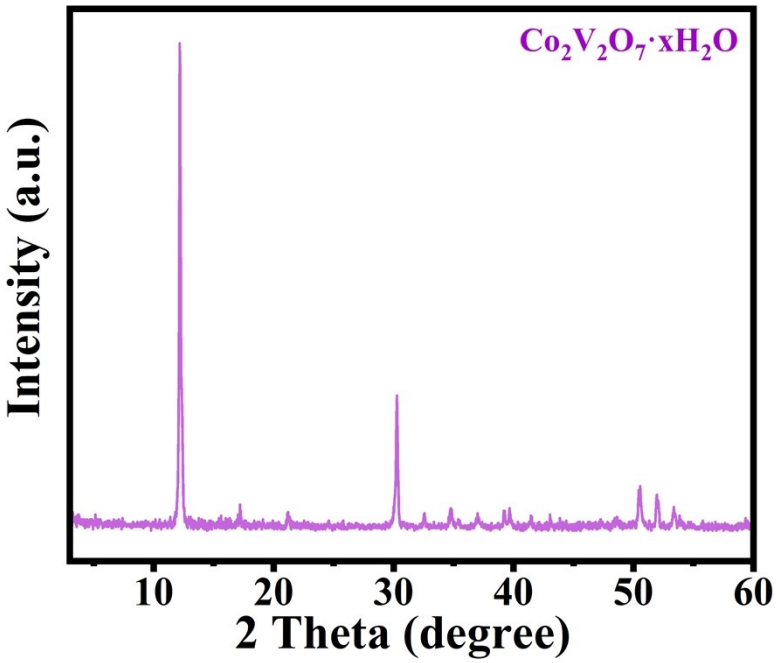

Fig. S2. Typical XRD pattern of the $Co_2V_2O_7$ precursor.

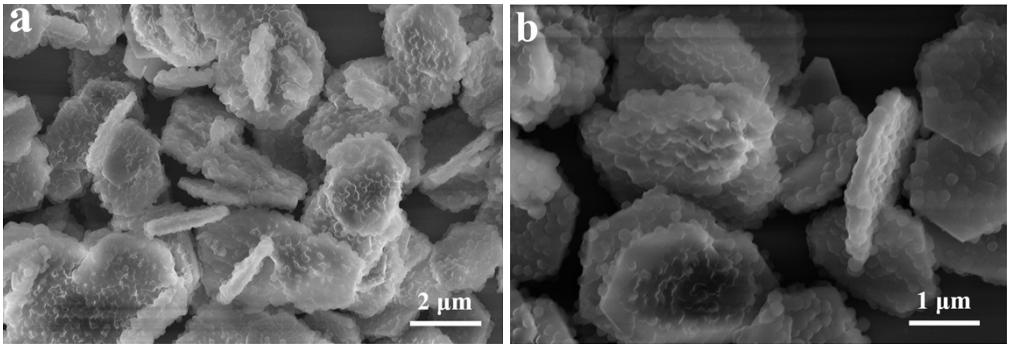

Fig. S3. SEM images of the core-shell $Co_2V_2O_7$@ZIF-8 heterostructure.

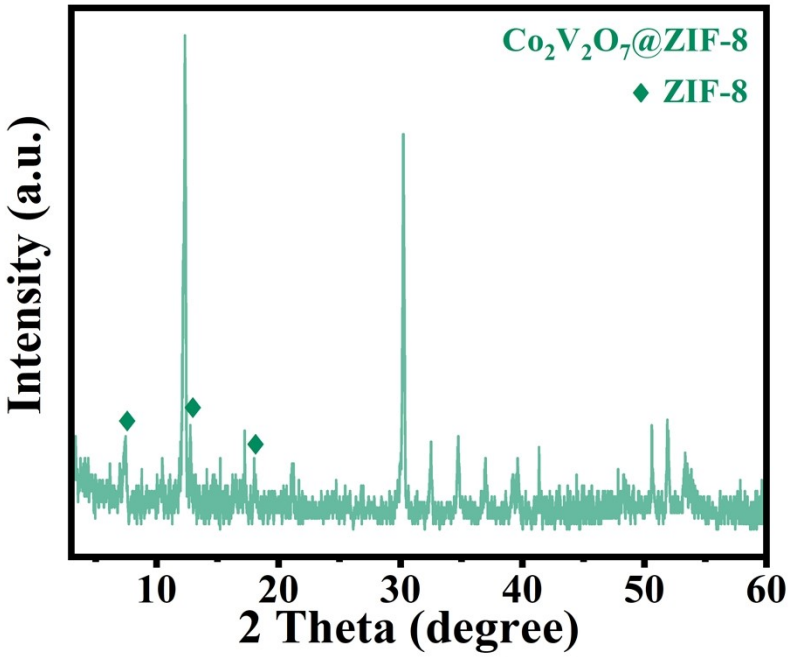

Fig. S4. Typical XRD pattern of the core-shell $Co_2V_2O_7$@ZIF-8 heterostructure.

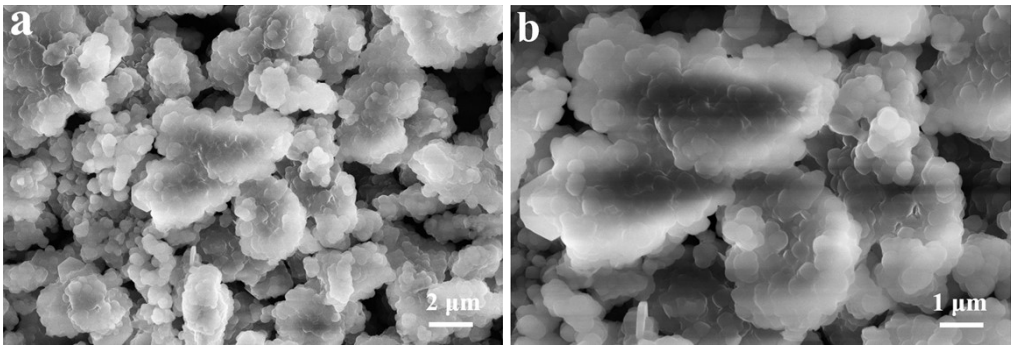

Fig. S5. SEM images of the ZIF-8 grown on $Co_2V_2O_7$ at 30 min.

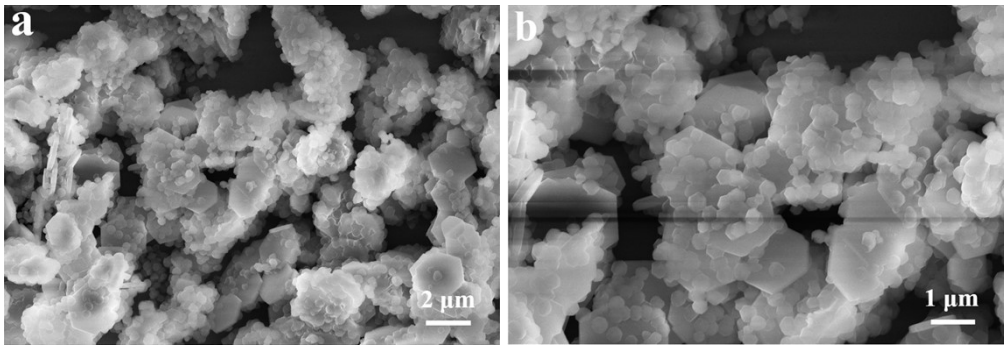

Fig. S6. SEM images of the ZIF-8 grown on $Co_2V_2O_7$ without addition of PVP.

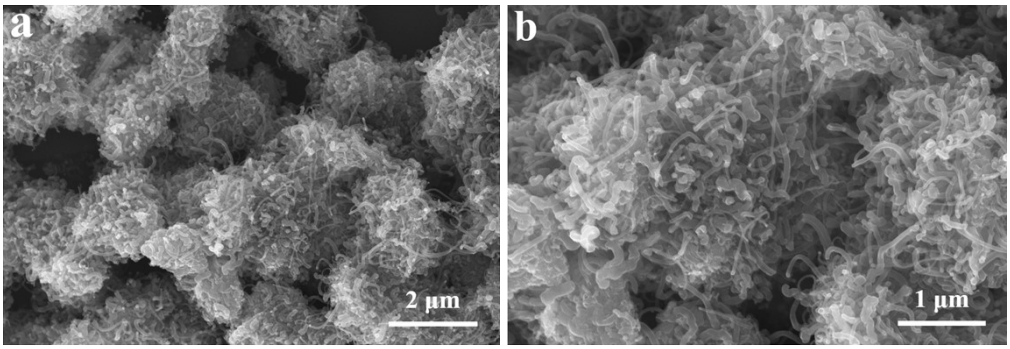

Fig. S7. SEM images of the VN/Co@NCNTs composite.

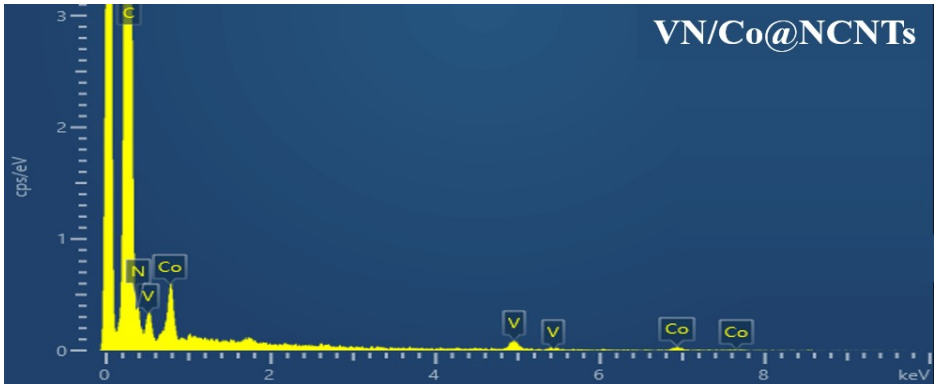

Fig. S8. EDS spectrum of the VN/Co@NCNTs composite.

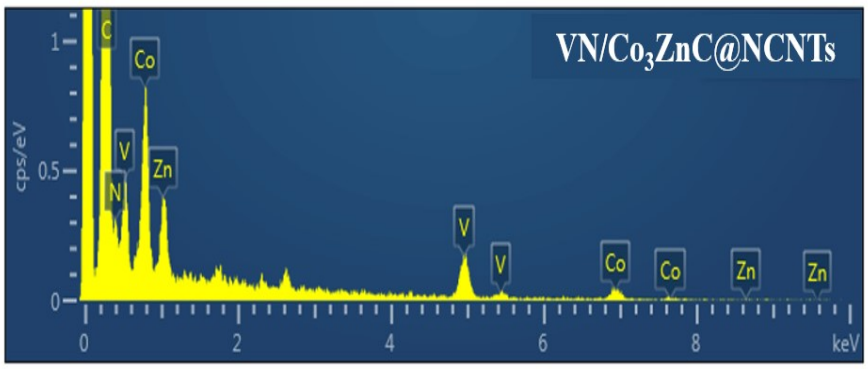

Fig. S9. EDS spectrum of the VN/Co_3ZnC@NCNTs composite.

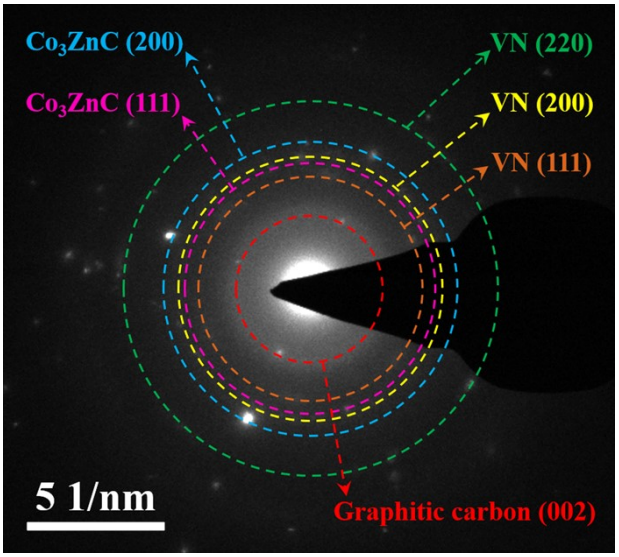

Fig. S10. SAED pattern of the VN/Co_3ZnC@NCNTs composite.

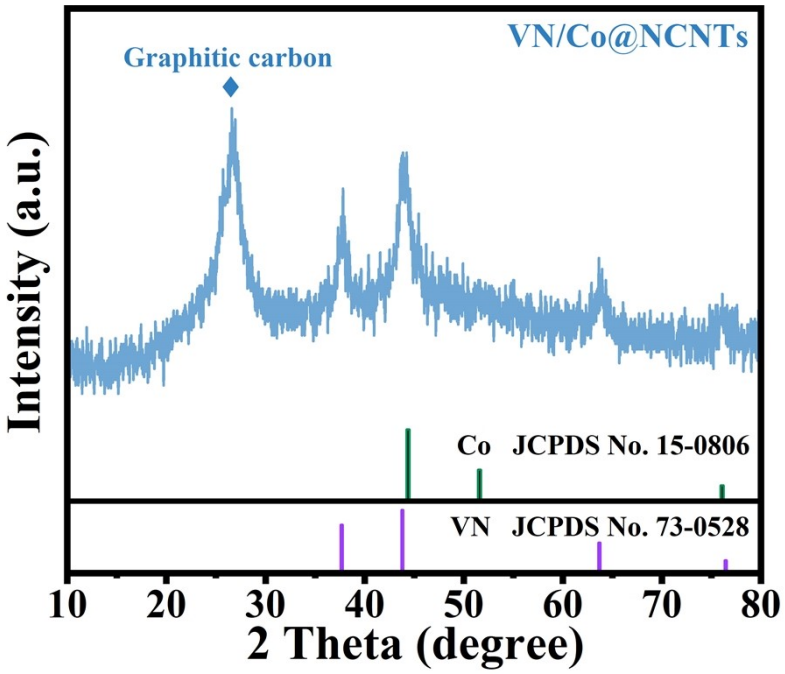

Fig. S11. Typical XRD pattern of the VN/Co@NCNTs composite.

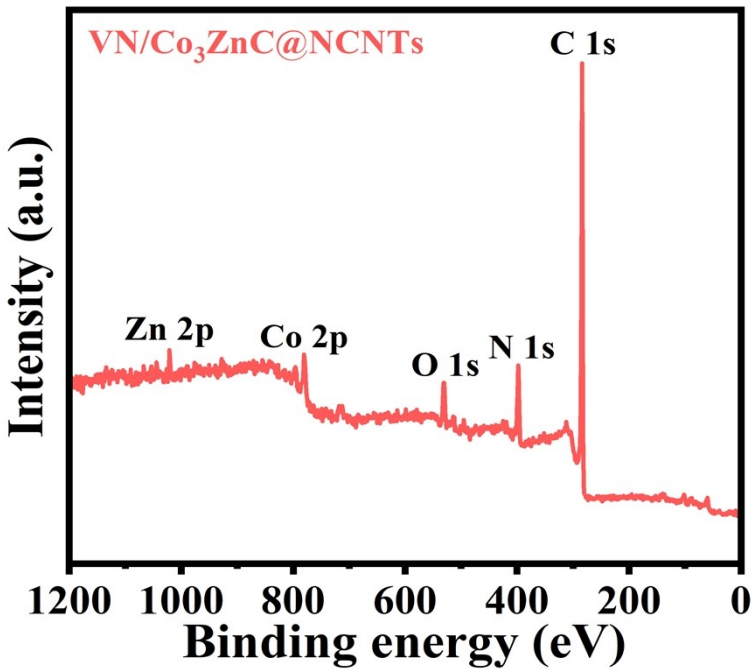

Fig. S12. Full XPS spectrum of the VN/Co_3ZnC@NCNTs composite.

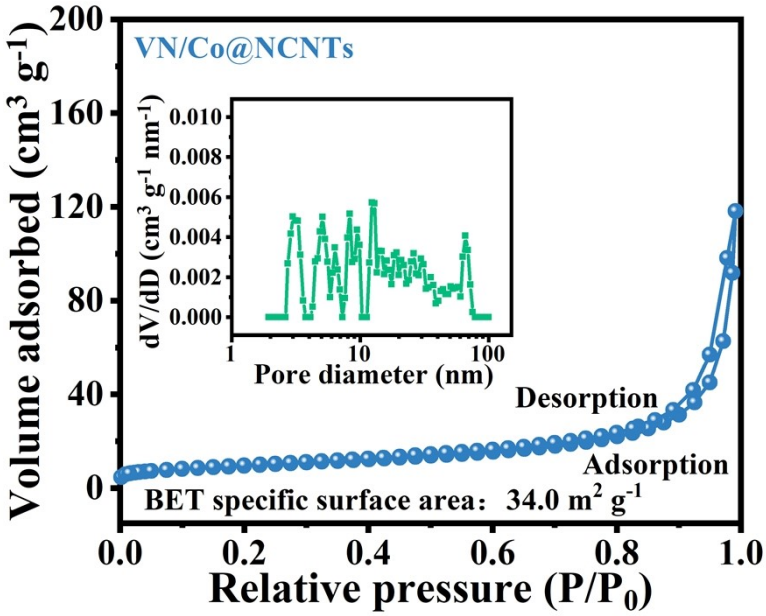

Fig. S13. N_2 adsorption-desorption isotherm curve of the VN/Co@NCNTs composite and the pore size distribution (inset).

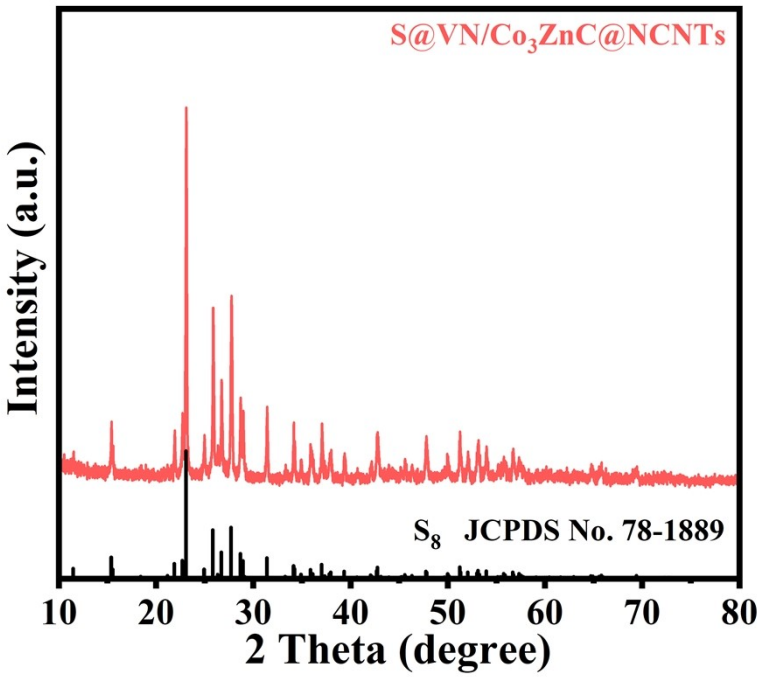

Fig. S14. XRD pattern of the VN/Co_3ZnC@NCNTs composite after sulfur loading.

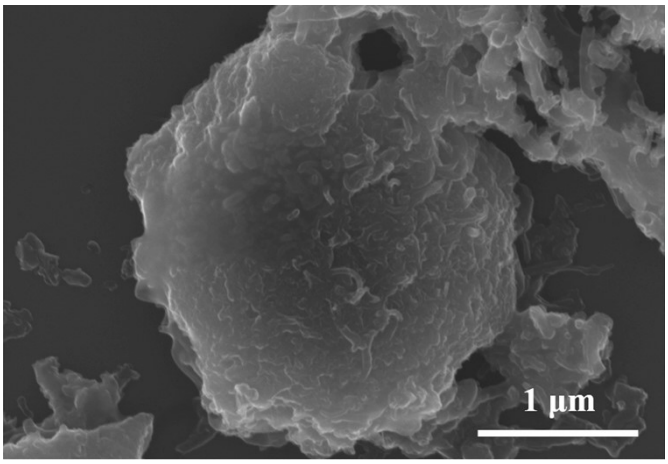

Fig. S15. SEM image of the S@VN/Co_3ZnC@NCNTs.

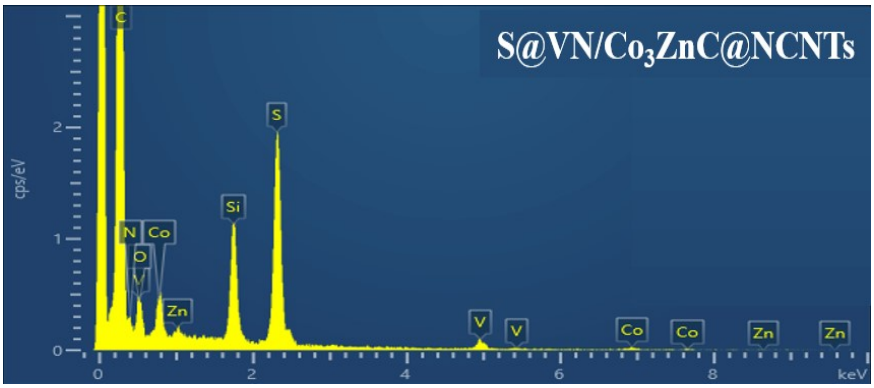

Fig. S16. EDS spectrum of the S@VN/Co_3ZnC@NCNTs.

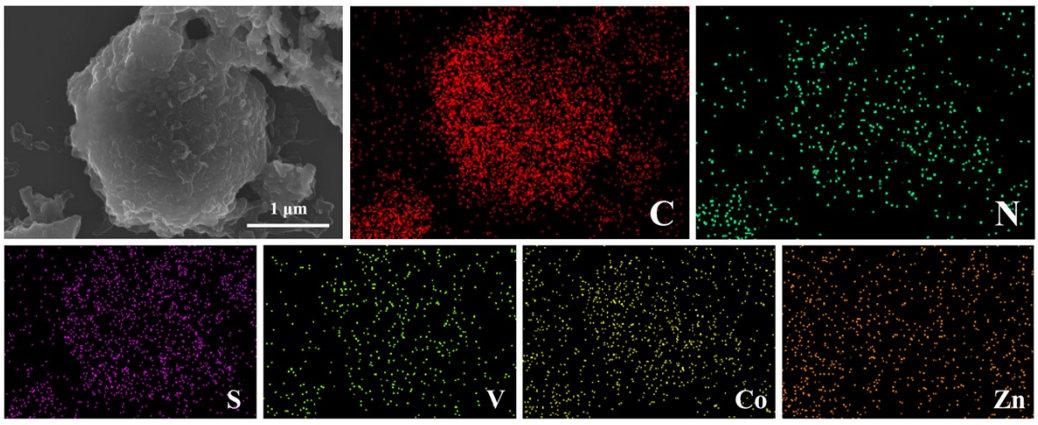

Fig. S17. EDS mapping images of the S@VN/Co_3ZnC@NCNTs.

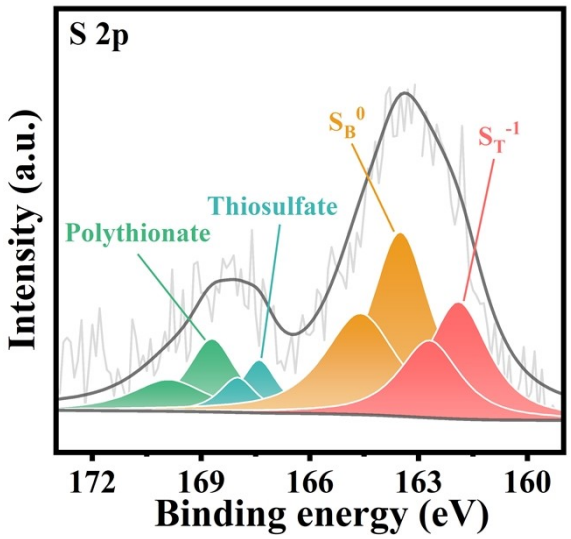

Fig. S18. S 2p spectrum of the VN/Co_3ZnC@NCNTs after Li_2S_6 adsorption.

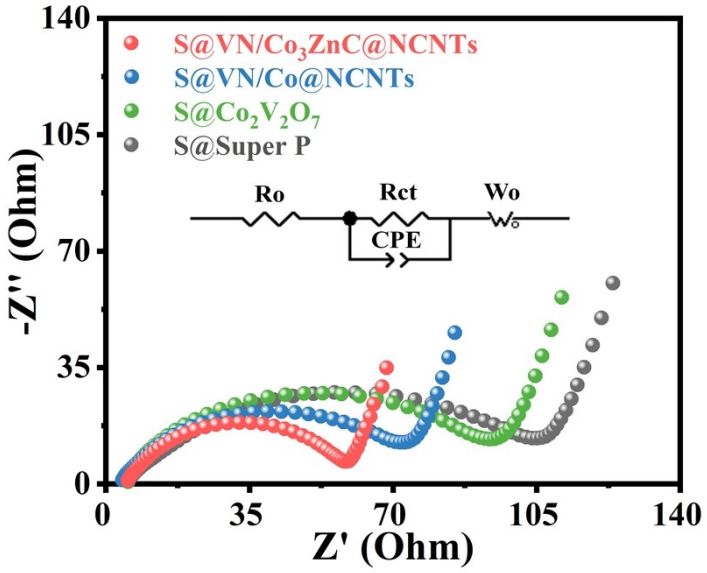

Fig. S19. Electrochemical impedance spectra of the S@VN/Co_3ZnC@NCNTs, S@VN/Co@NCNTs, S@$Co_2V_2O_7$ and S@Super P cathodes.

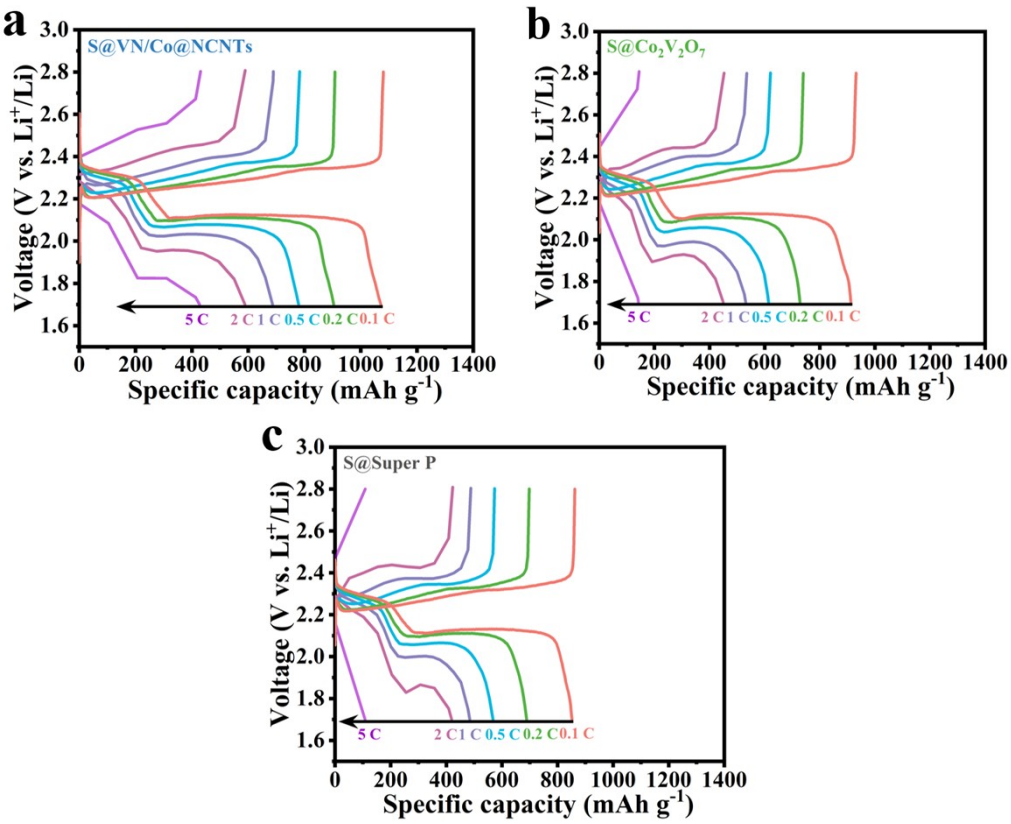

Fig. S20. GCD curves of the (a) S@VN/Co@NCNTs, (b) S@$Co_2V_2O_7$ and (c) S@Super P cathodes at different current densities ranged from 0.1 to 5 C, respectively.

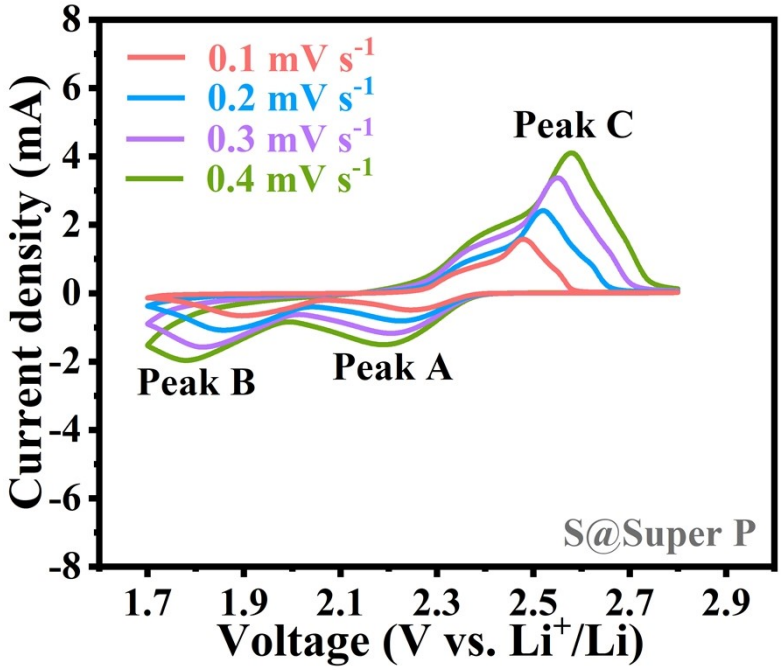

Fig. S21. CV curves of the S@Super P cathode at various scan rates.

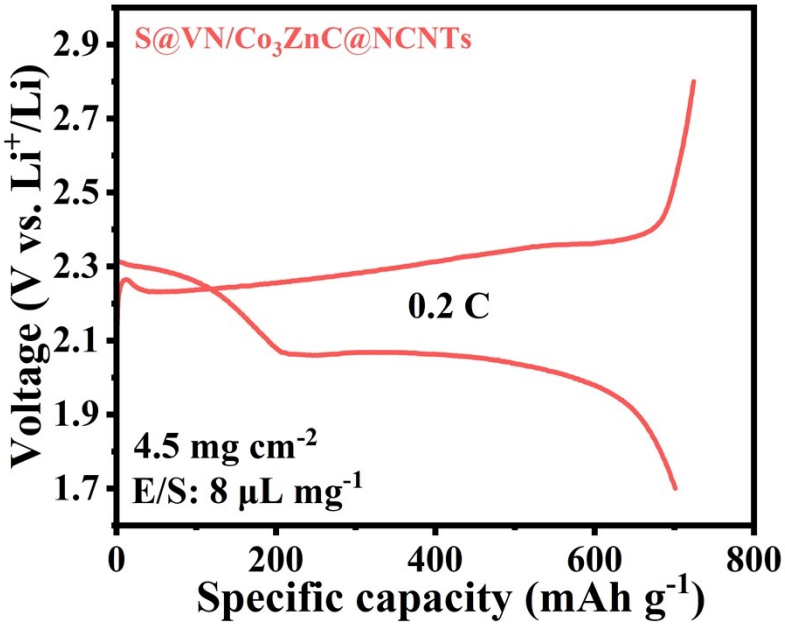

Fig. S22. GCD curves of the S@VN/Co_3ZnC@NCNTs cathode at 0.2 C with high sulfur loading (4.5 mg cm^{-2}).

Table S1. Comparison of the rate performance of VN/Co_3ZnC@NCNTs with other recently reported sulfur host materials.

Sulfur host	Capacity ($mAh\ g^{-1}$) (Low rate)	Capacity ($mAh\ g^{-1}$) (High rate)	Sulfur content (wt%)	Sulfur loading ($mg\ cm^{-2}$)	Ref.
VN@Co_3ZnC/NCNTs	**1399.4 (0.1 C)**	**624.4 (4 C) 566.4 (5 C)**	**50.0**	**1.0-1.2**	**This work**
N-HPCB	1065.0 (0.2 C)	535.0 (4 C)	49.0	1.1-1.5	10
GC-TiO@CHF	1100.0 (0.05 C)	620.0 (2 C)	58.4	—	11
CNT@TiO_{2-x}	1181.0 (0.1 C)	399.0 (5 C)	58.3	2.2	12
NiS_2-RGO	1385.0 (0.1 C)	304.0 (4 C)	—	5.0	13
MoN-VN	1436.0 (0.1 C)	636.0 (2 C)	58.5	1.13	20
TiO_2-TiN	1083.9 (0.2 C)	564.7 (4 C)	51.1	1.0	21
C@TiN	1149.0 (0.2 C)	373.0 (5 C)	49.7	1.1	28
CoNiP-rGO	954.9 (0.2 C)	598.2 (3 C)	42.0	1.5	49
V-N-C	1111.2 (0.5 C)	530.1 (5 C)	51.8	1.0	50
rGO-CNT-CoP(A)	1157.0 (0.2 C)	706.0 (3 C)	46.4	2.1	51
H-MoC-NC	1316.0 (0.1 C)	646.0 (3 C)	48.9	1.0-1.2	S1
C/Co_3O_4	1036.0 (0.1 C)	428.0 (3 C)	59.4	1.0	S2
N-CN-750@Co_3Se_4	1437.0 (0.1 C)	646.0 (3 C)	43.1	1.5	S3
H-TiO_x@S/PPy	1130.0 (0.1 C)	726.0 (1 C)	48.6	0.8-1.0	S4
Fe_3C/Fe_3N@NCNT	1224.0 (0.1 C)	653.0 (2 C)	49.8	2.0	S5
Mo_3Ni_3N/Mo_2C-CBC	1104.0 (0.1 C)	293.0 (5 C)	—	—	S6

Table S2. Comparison of the long-cycling capacity decay rate per cycle of S@VN/Co_3ZnC@NCNTs cathode with recently reported Li-S batteries.

Sulfur host	Rate (C)	Cycles	Capacity decay per cycle (%)	Sulfur content (wt%)	Sulfur loading (mg cm^{-2})	Ref.
VN/Co_3ZnC@NCNTs	**1**	**500**	**0.064**	**50.0**	**1.0-1.2**	**This work**
MoN-VN	2	500	0.068	58.5	1.1	20
3DNG/TiN	1	200	0.177	—	—	25
CoNiP-rGO	1	600	0.080	42.0	1.5	49
V–N–C	1	500	0.087	51.8	1.0	50
rGO-CNT-CoP(A)	2	200	0.090	46.4	2.1	51
MVN@C NWs	1	200	0.194	57.2	—	52
OCN-900	0.5	500	0.100	39.2	—	53
NbN@NG	1	400	0.090	49.6	2.4	54
CoS_2@NGCNs	1	300	0.075	—	1.1-1.5	55
In_2S_{3-x}/rGO-Li_2S_6	0.5	450	0.123	—	1.0	56
rGO@mC-MnO-800	1	250	0.160	49.6	1.5	57
TiN@graphene	0.5	200	0.176	63.4	0.8	58

Table S3. Lithium-ion diffusion rates (D_{Li+}, $cm^2\ s^{-1}$) of the Li-S batteries with different cathodes.

Sample	Peak A	Peak B	Peak C
S@VN/Co_3ZnC@NCNTs	4.91×10^{-8}	1.55×10^{-7}	2.53×10^{-7}
S@VN/Co@NCNTs	2.55×10^{-8}	6.00×10^{-8}	1.05×10^{-7}
S@$Co_2V_2O_7$	1.24×10^{-8}	3.66×10^{-8}	6.55×10^{-8}
S@Super P	0.65×10^{-8}	2.47×10^{-8}	5.40×10^{-8}

Table S4. Comparison of the high-sulfur-loading performance of VN/Co_3ZnC@NCNTs cathode with other recently reported sulfur host materials.

Sulfur host	Sulfur loading (mg cm^{-2})	Capacity (mAh g^{-1})	Ref.
VN@Co_3ZnC/NCNTs	**4.5**	**639.2 (100^{th} cycle at 0.2 C)**	**This work**
N-PC@uCo	3.8	535.0 (200^{th} cycle at 0.5 C)	15
Hollow TiO_2-TiN	3.0	610.8 (100^{th} cycle at 0.3 C)	21
VN-NBs	6.8	563.0 (200^{th} cycle at 0.5 C)	22
Ti_4O_7/TiN/C	3.0	~530.0 (300^{th} cycle at 1 C)	30
CoNiP-rGO	6.0	421.7 (100^{th} cycle at 0.1 C)	49
In_2S_{3-x}/rGO-Li_2S_6	4.0	539.0 (50^{th} cycle at 0.1 C)	56
TiN@graphene	3.6	515.0 (200^{th} cycle at 1 C)	58
Mo_2C-Mo_3N_2/rGO	5.0	486.0 (300^{th} cycle at 0.5 C)	59
Co-SAs@NC	5.0	~400.0 (150^{th} cycle at 1 C)	60
Co/CoP@NC	4.9	~320.4 (100^{th} cycle at 1 C)	61
TiC@C-TiO_2	2.3	603.0 (160^{th} cycle at 0.5 C)	62
G-VS_2	3.5	520.0 (150^{th} cycle at 1 C)	63
Mo_2C-C NOs	4.2	623.0 (100^{th} cycle at 0.5 C)	64
Co_9S_8	4.5	~555.6 (150^{th} cycle at 0.2 C)	S7
CNTs-COOH@hemin	6.5	530.7 (200^{th} cycle at 0.1 C)	S8
Mn/C-(N, O)	4.0	525.0 (100^{th} cycle at 1 C)	S9
PRC/Ni	4.0	563.8 (200^{th} cycle at 0.2 C)	S10

Reference

S1 W. Deng, Z. Xu, Z. Deng and X. Wang, *J. Mater. Chem. A*, 2021, **9**, 21760−21770.

S2 F. Ma, J. Liang, T. Wang, X. Chen, Y. Fan, B. Hultman, H. Xie, J. Han, G. Wu and Q. Li, *Nanoscale*, 2018, **10**, 5634−5641.

S3 D. Cai, B. Liu, D. Zhu, D. Chen, M. Lu, J. Cao, Y. Wang, W. Huang, Y. Shao, H. Tu and W. Han, *Adv. Energy Mater.*, 2020, **10**, 1904273.

S4 G. Chen, W. Zhong, Y. Li, Q. Deng, X. Ou, Q. Pan, X. Wang, X. Xiong, C. Yang and M. Liu, *ACS Appl. Mater. Interfaces*, 2019, **11**, 5055−5063.

S5 T. Zhu, Y. Sha, H. Zhang, Y. Huang, X. Gao, M. Ling and Z. Lin, *ACS Appl. Mater. Interfaces*, 2021, **13**, 20153−20161.

S6 Y.-S. Liu, Y.-L. Bai, X. Liu, C. Ma, X.-Y. Wu, X. Wei, Z. Wang, K.-X. Wang and J.-S. Chen, *Chem. Eng. J.*, 2019, **378**, 122208.

S7 Q. Pang, D. Kundu and L. F. Nazar, *Mater. Horiz.*, 2016, **3**, 130−136.

S8 X. Ding, S. Yang, S. Zhou, Y. Zhan, Y. Lai, X. Zhou, X. Xu, H. Nie, S. Huang and Z. Yang, *Adv. Funct. Mater.*, 2020, **30**, 2003354.

S9 Y. Liu, Z. Wei, B. Zhong, H. Wang, L. Xia, T. Zhang, X. Duan, D. Jia, Y. Zhou and X. Huang, *Energy Storage Mater.*, 2021, **35**, 12−18.

S10 Y. Zhong, X. Xia, S. Deng, J. Zhan, R. Fang, Y. Xia, X. Wang, Q. Zhang and J. Tu, *Adv. Energy Mater.*, 2018, **8**, 1701110.